


Article

Twins in $\text{YAl}_3(\text{BO}_3)_4$ and $\text{K}_2\text{Al}_2\text{B}_2\text{O}_7$ Crystals as Revealed by Changes in Optical Activity

Johannes Buchen ^{1,2} , Volker Wesemann ^{1,*}, Steffen Dehmelt ^{1,3}, Andreas Gross ¹ and Daniel Rytz ¹

¹ FEE GmbH, Struthstr. 2, 55743 Idar-Oberstein, Germany; jobuchen@caltech.edu (J.B.); sdehmelt@gmx.de (S.D.); gross@fee-io.de (A.G.); rytz@fee-io.de (D.R.)

² Division of Geological and Planetary Sciences, California Institute of Technology, 1200 E. California Blvd., Pasadena, CA 91125, USA

³ Hochschule Trier, Umwelt-Campus Birkenfeld, Campusallee, 55768 Hoppstädten-Weiersbach, Germany

* Correspondence: wesemann@fee-io.de

Received: 7 December 2018 ; Accepted: 20 December 2018; Published: 22 December 2018

Abstract: Many borate crystals feature nonlinear optical properties that allow for efficient frequency conversion of common lasers down into the ultraviolet spectrum. Twinning may degrade crystal quality and affect nonlinear optical properties, in particular if crystals are composed of twin domains with opposing polarities. Here, we use measurements of optical activity to demonstrate the existence of inversion twins within single crystals of $\text{YAl}_3(\text{BO}_3)_4$ (YAB) and $\text{K}_2\text{Al}_2\text{B}_2\text{O}_7$ (KABO). We determine the optical rotatory dispersion of YAB and KABO throughout the visible spectrum using a spectrophotometer with rotatable polarizers. Space-resolved measurements of the optical rotation can be related to the twin structure and give estimates on the extent of twinning. The reported dispersion relations for the rotatory power of YAB and KABO may be used to assess crystal quality and to select twin-free specimens.

Keywords: NLO crystals; frequency conversion; second harmonic generation; YAB; $\text{YAl}_3(\text{BO}_3)_4$; KABO; $\text{K}_2\text{Al}_2\text{B}_2\text{O}_7$; optical activity; optical rotatory dispersion; inversion twin

1. Introduction

A series of borates with the general formula $\text{RAl}_3(\text{BO}_3)_4$ ($R = \text{Y}$ or rare earth element (REE)) adopts the crystal structure of the carbonate mineral huntite, $\text{CaMg}_3(\text{CO}_3)_4$ [1–3]. In this structure type, the coplanar arrangement of $[\text{BO}_3]^{3-}$ groups amplifies the intrinsic nonlinear dielectric susceptibility of the $[\text{BO}_3]^{3-}$ group and combines it with strong birefringence and a spectral transparency that extends into the ultraviolet (UV) region [4–6]. $\text{YAl}_3(\text{BO}_3)_4$ (YAB) is transparent down to about 170 nm [7,8] and shows an acceptable effective nonlinear optical (NLO) coefficient [9]. The refractive indices of YAB permit phase matching for several types of frequency conversion to UV light including second harmonic generation (SHG) from 532 nm to 266 nm [7–9]. In contrast to many other NLO borates, YAB is non-hygroscopic and hard (Mohs hardness 7.5 [2]) as compared to $\beta\text{-BaB}_2\text{O}_4$ (BBO) [10], LiB_3O_5 (LBO) [11], and $\text{CsLiB}_6\text{O}_{10}$ (CLBO) [12]. Albeit not a huntite borate, the material $\text{K}_2\text{Al}_2\text{B}_2\text{O}_7$ (KABO) shares many of the advantages of YAB [13,14]. Both YAB and KABO are free of toxic elements, such as beryllium, an essential component of other proposed NLO materials including $\text{Sr}_2\text{Be}_2\text{B}_2\text{O}_7$ (SBBO) [15] and $\text{KBe}_2\text{BO}_3\text{F}_2$ (KBBF) [16,17]. The combinations of suitable optical, chemical, and mechanical properties turn YAB and KABO into promising crystals for NLO applications in the UV spectral region.

Both pure and REE-doped YAB crystals, however, typically show a lamellar microstructure as revealed by X-ray diffraction topography [18], surface etching patterns [19,20], and atomic force microscopy [21]. A similar microstructure has been detected in crystals of the borate huntite $\text{Y}_{0.57}\text{La}_{0.72}\text{Sc}_{2.71}(\text{BO}_3)_4$ (YLSB) [22,23]. Based on these observations, the lamellae have been interpreted

as polysynthetic inversion twins with reflection on $\{11\bar{2}0\}$ planes as the twin operation and adjacent twin domains sharing planes parallel to $\{10\bar{1}1\}$ [18,21,24]. This twin law, i.e., reflection on $\{11\bar{2}0\}$ with domain boundaries parallel to $\{10\bar{1}1\}$, also describes Brazil twins in low-quartz (α -SiO₂) (e.g., [25,26]). Similar twins involving reflection on planes perpendicular to the crystallographic *a* axis, like $\{11\bar{2}0\}$, have also been suggested for SBBO [27], which is structurally similar to KABO [13,14]. Note that for the space groups of YAB (*R*32 [1]), KABO (*P*321 [13]), and low-quartz (*P*3₁21), these twin laws generate merohedral twins [24] (twinning by merohedry [28]) that are not readily detected by conventional X-ray diffraction techniques. As these space groups share the same acentric and enantiomorphous crystal class (32), however, reflecting the crystal structure on planes perpendicular to the *a* axes not only inverts the polar two-fold axes along *a* but also converts the right-handed polytype of each structure into its left-handed counterpart and vice versa.

The domain structures of Yb:YAB and Nd:YAB have been shown to severely affect the SHG output at 532 nm by partially back-converting second harmonic light along interfaces between domains of opposing polarity [29,30]. Stacks of periodically inverted polar domains can, however, convert light to higher harmonics via quasi-phase-matching [31] as experimentally demonstrated using, for example, artificially twinned low-quartz crystals [32,33]. Indeed, accidental quasi-phase-matching has also been observed in Yb:YAB and Nd:YAB crystals with as-grown twin domains of suitable shape [29,30]. For crystals of class 32, inversion twins also affect the optical activity of twinned crystals as right- and left-handed domains rotate the electric field vector in opposing senses. To relate an observed optical rotation to inversion twinning, however, the unaffected or intrinsic rotatory power of the crystal species needs to be known. We determined the intrinsic rotatory powers of YAB and KABO as a function of the wavelength using a spectrophotometer with rotatable polarizers and applied the results to characterize the intracrystalline microstructure of these borates. Within individual YAB and KABO crystals, we found changes in the sign and magnitude of the optical rotation revealing inversion twins composed of right- and left-handed domains.

2. Materials and Methods

2.1. Crystal Growth and Sample Preparation

YAB crystals were grown by the top-seeded solution growth (TSSG) technique from YAB solutions based on the solvent systems Li₂O–WO₃–B₂O₃ [34] and Li₂O–Al₂O₃–B₂O₃ [8]. Depending on the solvent, the habitus of the YAB crystals varied between stubby and prismatic with the positive rhombohedron $\{10\bar{1}1\}$ and the trigonal prisms $\{11\bar{2}0\}$ and $\{\bar{1}\bar{1}20\}$ as dominating crystal faces. In all YAB crystals, a central zone of inclusions extended along the pulling direction. A KABO crystal was synthesized by TSSG from a NaF solution [35,36] with a small excess of B₂O₃. The crystal did not develop flat crystal faces and contained polycrystalline regions similar to previous reports on KABO crystals grown from NaF flux [36]. Platelets with an orientation approximately perpendicular to the trigonal symmetry axis (crystallographic *c* axis) were cut from YAB and KABO crystals and ground down close to designated thicknesses using alumina powder. The platelets were then oriented perpendicular to the *c* axis to better than 9° using X-ray diffraction in a Laue backscattering geometry and double-sided polished to plane-parallel sections using colloidal silica slurry. Section thicknesses were determined with a digital micrometer giving an accuracy of about 0.005 mm.

2.2. Measurement of the Rotatory Power at Different Wavelengths

In an optically active crystal, an incident linearly polarized light wave splits into two elliptically polarized waves with opposite senses of rotation, left (L) and right (R), that propagate through the crystal with different velocities according to their refractive indices n_L and n_R . At each point along the propagation path through the crystal, the different wavelengths of the two elliptically polarized waves give rise to a phase shift 2ϕ between the angles by which the dielectric displacement vectors of the two waves have been rotated. The phase shift 2ϕ is proportional to the difference in refractive indices

and increases with the optical path length L through the crystal. As a result, the polarization of the combined wave that leaves the crystal is rotated by an angle ϕ with respect to the polarization of the incident light wave (e.g., [37,38]):

$$\phi = \frac{\pi(n_L - n_R)L}{\lambda} \quad (1)$$

where λ is the wavelength of the light wave outside the crystal. The rotatory power or specific rotation is defined as [39]:

$$\rho = \phi/L = \frac{\pi(n_L - n_R)}{\lambda} \quad (2)$$

For the definition of the sense of rotation and the sign of the rotatory power, see the standard reference by Glazer and Stadnicka [39]. YAB, KABO, and low-quartz are optically uniaxial, and we focus here on the optical activity for light propagation along the optical axis, i.e., parallel to the crystallographic c axis.

To measure the angle of rotation ϕ as a function of wavelength λ , we used a PerkinElmer Lambda 1050 spectrophotometer equipped with rotatable calcite polarizers. A schematic draft of the setup is shown in Figure 1a. Polychromatic light emitted by deuterium ($\lambda < 320$ nm) and tungsten ($\lambda > 320$ nm) lamps was sent through a double-stage monochromator based on holographic gratings and polarized by a motorized rotatable polarizer. A series of apertures was used to collimate the light beam to an effective aperture of about 1 mm on the crystal surface. The light was transmitted through the plane-parallel crystal section and through a second polarizer placed behind the crystal, the analyzer, and was detected with a photomultiplier ($\lambda < 820$ nm) or an InGaAs photodiode ($\lambda > 820$ nm). Polarizers were crossed by setting the rotation angle of the first polarizer to $\psi = 0$ and by manually rotating the analyzer so as to minimize the transmitted intensity. We crossed the polarizers for a wavelength of $\lambda = 1100$ nm to avoid bias by ambient light that might have entered the spectrophotometer during the alignment procedure.

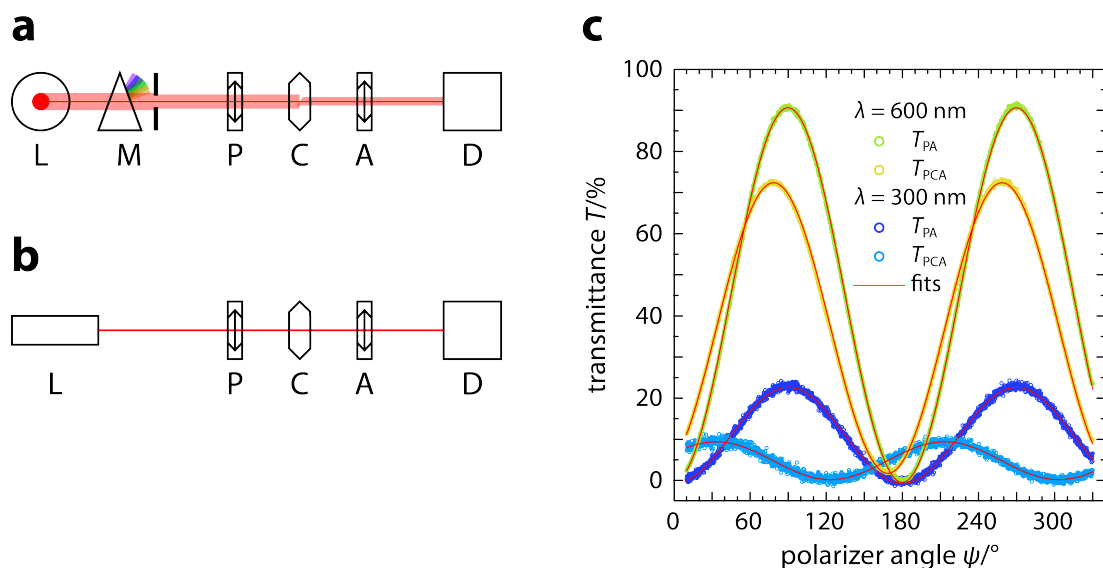


Figure 1. Experimental setup for the measurement of the optical rotatory power. (a,b) Arrangement of optical components in the spectrophotometer and for a setup using a laser as the light source. L: light source (deuterium or tungsten lamp in (a) and He-Ne laser in (b)), M: monochromator, P: rotatable polarizer, C: optically active crystal, A: rotatable analyzer, D: detector. (c) Transmittance through polarizer and analyzer (PA) and through polarizer, YAB crystal, and analyzer (PCA) recorded with the spectrophotometer as a function of the polarizer angle.

At a given wavelength, the polarizer angle ψ was scanned from 10° to 330° in steps of 0.15° and the light intensity T_{PCA}^* transmitted through polarizer (P), crystal (C), and analyzer (A) was recorded for 0.2 s at each step. Then, the crystal was removed from the beam path and the scan was repeated to measure the light intensity T_{PA}^* transmitted through polarizer and analyzer only. Transmitted light intensities T^* were recorded as transmittances relative to a reference beam path and were corrected for the inherent polarization of the incident beam and potential polarization-dependent sensitivities of the detectors using an additional polarization scan with only the polarizer in the beam path (T_{P}^*). Observed transmittances T^* were corrected as follows:

$$T_{\text{PCA}} = \frac{T_{\text{PCA}}^* - \langle T_0^* \rangle}{T_{\text{P}}^* - \langle T_0^* \rangle} \quad \text{and} \quad T_{\text{PA}} = \frac{T_{\text{PA}}^* - \langle T_0^* \rangle}{T_{\text{P}}^* - \langle T_0^* \rangle} \quad (3)$$

where $\langle T_0^* \rangle$ is the mean transmittance for a polarization scan with the beam path blocked. Figure 1c shows the corrected transmittances T_{PCA} through a YAB crystal at 600 nm and 300 nm as a function of the polarizer angle ψ together with the corrected transmittance scans $T_{\text{PA}}(\psi)$ without the crystal section.

For each wavelength, the corrected transmittance scans $T_{\text{PCA}}(\psi)$ and $T_{\text{PA}}(\psi)$ were fit to functions of the form

$$T(\psi) = \Delta T \sin^2(\psi - \epsilon) + T(\epsilon) \quad (4)$$

with the polarizer extinction angle ϵ at which the transmittance is reduced to the minimum value $T(\epsilon)$ of the respective scan. ΔT measures the amplitude of the variation in transmittance along a polarization scan. Note that the three parameters ϵ , $T(\epsilon)$, and ΔT are constrained by more than 2000 data points of each transmittance scan. The angle ϕ by which the plane of polarization of the incident light beam is rotated by the optically active crystal is equal to the absolute difference $|\epsilon_{\text{PCA}} - \epsilon_{\text{PA}}|$. Accordingly, the magnitude of the rotatory power is given as

$$|\rho| = |\epsilon_{\text{PCA}} - \epsilon_{\text{PA}}|/L. \quad (5)$$

To determine the optical rotatory dispersion $\rho(\lambda)$, the measurements and analysis were repeated as described above for incident light of different wavelengths between 300 nm and 900 nm. Based on repeated measurements at the same wavelength, we estimate observed rotatory powers to be reproducible within $0.1^\circ \text{ mm}^{-1}$.

Our approach of measuring the optical rotation angle as a function of wavelength shares some similarities with recently reported methods that are either based on channeled spectra recorded using a spectrophotometer with crossed polarizers [40,41] or that employ a motorized rotatable analyzer followed by a transmission grating to disperse the light onto a linear CCD array for simultaneous detection over a range of wavelengths [42]. Here, we combined the high spectral resolution and wide spectral range of the spectrophotometer with the high angular precision provided by polarization scans. By following the procedure outlined above, the transmission properties of a given pair of polarizers are readily calibrated without need to accurately cross them by hand.

2.3. Space-Resolved Measurements of the Optical Rotation

To detect potential variations in optical rotation within individual crystals, plane-parallel crystal sections were mounted onto a three-axis stage and aligned with their polished faces perpendicular to the beam of a He-Ne laser with 2 mW output power. Rotatable Glan-Thompson polarizers were placed in the beam path before (polarizer) and after (analyzer) the crystal section. Light transmitted through the polarizer, crystal, and analyzer was detected with a power meter. Figure 1b shows a scheme of the setup. The analyzer extinction angle ϵ was determined with and without the crystal section in the beam path by manually rotating the analyzer so as to minimize the transmitted light intensity by reading off the angle from the vernier scale on the analyzer mount. Again, the difference $|\epsilon_{\text{PCA}} - \epsilon_{\text{PA}}|$ equals the angle ϕ by which the crystal rotates the plane of polarization of the laser. By moving the crystal with the three-axis stage, the rotation angle ϕ was measured at different positions through the

crystal section. The diameter of the laser beam limited the lateral spatial resolution to about 1 mm. Repeated measurements that aimed to reproduce both the position on the crystal section as well as the extinction angle ϵ at that position showed the observed rotation angles ϕ to be precise within 0.1° .

3. Results

3.1. Low-Quartz, α -SiO₂

An oriented low-quartz crystal with plane-parallel polished faces perpendicular to the crystallographic c axis and a thickness of 4.817(5) mm served as a reference to assess the accuracy of our measurements of the rotatory power at different wavelengths using the spectrophotometer. Figure 2 compares our results with previous measurements [43] and calculations [44] of the rotatory power of low-quartz. We described the optical rotatory dispersion using a semi-empirical formalism based on the theory of circular dichroism [39,45]:

$$\rho = A/(\lambda^2 - \lambda_1^2). \quad (6)$$

The constant A captures the strength of dispersion, while λ_1 is the wavelength of an optically active electronic transition [39]. While more elaborate formulations for the optical rotatory dispersion of low-quartz have been proposed [45–47], we found the simple expression (6) to accurately describe our experimental data within their uncertainties. By fitting Equation (6) to our experimental results, we obtained $A = 7.17(3)^\circ \text{ mm}$ and $\lambda_1 = 129(1) \text{ nm}$. Inter- and extrapolating our results using these parameters in the dispersion relation (6) gave excellent agreement with literature data on the rotatory power of low-quartz, even at wavelengths in the deep UV where the rotatory power is strongly affected by dispersion and outside the spectral range accessible with the spectrophotometer (Figure 2). This result demonstrates the accuracy of our method to determine the rotatory power at different wavelengths using a spectrophotometer.

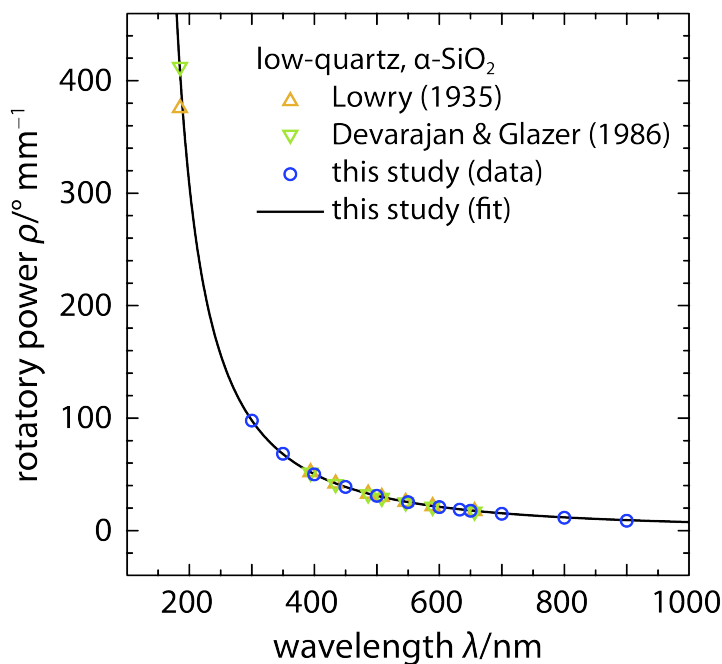


Figure 2. Optical rotatory dispersion of low-quartz, α -SiO₂. Lowry (1935): measurements [43]; Devarajan & Glazer (1986): calculation [44]; this study: measurements and fit to data.

3.2. YAB, $YAl_3(BO_3)_4$

In the case of YAB, the measurement of the rotatory power is complicated by inversion twins that might reduce the observed rotatory power to values below the intrinsic rotatory power. When a light wave traverses a sequence of left- and right-handed domains, their individual contributions to the observed optical rotation angle ϕ will partly cancel each other out and thereby result in underestimation of the rotatory power. We searched for a YAB crystal containing a large tentative single domain that provided the longest possible optical path length along the *c* axis. We then measured the optical rotation angle through this domain at different wavelengths. The crystal was then reground and polished to shorten the optical path length along the *c* axis without changing the crystal orientation, and the measurement of the optical rotation angle was repeated. In total, we measured optical rotation angles at 11 different wavelengths for five different optical path lengths on the same domain. In case the domain contained any twin lamellae with opposite senses of rotation, every change in the optical path length should have changed the relative proportions of left- and right-handed domains along the optical path and hence, the observed rotatory power. For the selected domain, we did not observe significant changes of the rotatory power when the optical path length changed.

Figure 3a shows the measured optical rotation angles ϕ for different wavelengths as a function of the optical path length L . For a given wavelength, the observed rotation angles display a linear relation with the optical path length. In particular, the highest rotation angles are observed for the longest optical path lengths. These observations suggest that the probed crystal volume was composed of a single domain and that the observed rotation angles were not affected by lamellae of inversion twins. To extract the dispersion relation of the rotatory power of YAB, we analyzed the complete data set of pairs of rotation angles ϕ and optical path lengths L using a modified version of Equation (6):

$$\phi = AL/(\lambda^2 - \lambda_1^2). \quad (7)$$

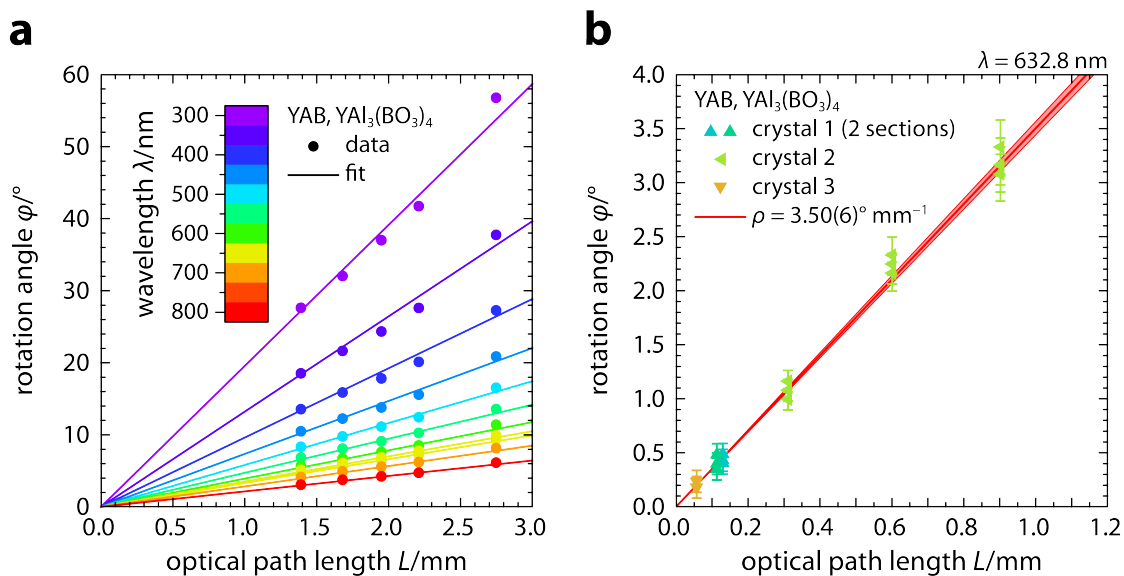


Figure 3. Optical rotation angles of YAB measured on domains with different optical path lengths. In (a), the lines show the result of simultaneously fitting a dispersion relation to the observed rotation angles at all wavelengths and path lengths shown in (a). The red line in (b) shows the fitting result of (a) for a wavelength of 632.8 nm. The shading indicates propagated uncertainties on fitted parameters. Note the linear relation between observed rotation angles and path lengths in (a) and the agreement of the fit with measurements at 632.8 nm on very thin domains in (b).

A fit to all data in Figure 3a gave $A = 1.32(2)^\circ \text{ mm}$ and $\lambda_1 = 149(4) \text{ nm}$. The corresponding dispersion curve is shown in Figure 4 together with rotatory powers, as calculated from the observed rotation angles.

To consolidate the results on the rotatory power of YAB obtained from measurements on a single large domain using the spectrophotometer, we searched for single domains of suitable size to be probed using the experimental setup with a He-Ne laser as the light source (see Section 2.3 and Figure 1b). The combination of the spatially confined laser beam with the three-axis stage allowed us to precisely navigate to and determine the optical rotation angles on small crystal volumes. Figure 3b compiles the results of measurements on single domains distributed over four crystal sections that were cut from three different YAB crystals. Note the good agreement between measurements on small domains with short optical path lengths using the laser setup and those on the large domain performed with the spectrophotometer. At the wavelength of the He-Ne laser ($\lambda = 632.8 \text{ nm}$), the parametrization of the dispersion relation of YAB derived above gives an optical rotatory power of $\rho(632.8 \text{ nm}) = 3.50(6)^\circ \text{ mm}^{-1}$.

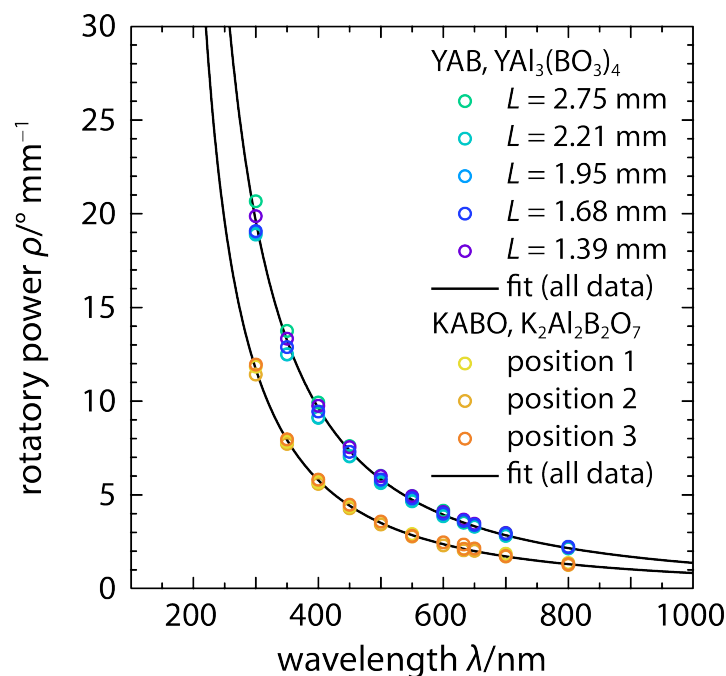


Figure 4. Optical rotatory dispersion of YAB ($\text{YAAl}_3(\text{BO}_3)_4$) and KABO ($\text{K}_2\text{Al}_2\text{B}_2\text{O}_7$). For YAB, rotatory powers were measured on the same domain for five different optical path lengths (see also Figure 3a). For KABO, rotatory powers were measured at three different locations on the same crystal section.

3.3. KABO, $\text{K}_2\text{Al}_2\text{B}_2\text{O}_7$

The rotatory power of a KABO crystal with a thickness of $0.717(5) \text{ mm}$ was measured along the *c* axis at 11 different wavelengths and at three different locations. The results are shown in Figure 4 together with the rotatory powers of YAB. Analysis of the KABO data with Equation (6) gave $A = 0.80(1)^\circ \text{ mm}$ and $\lambda_1 = 148(3) \text{ nm}$. Based on this dispersion relation, KABO rotates the plane of polarization by $2.10(3)^\circ \text{ mm}^{-1}$ at a wavelength of $\lambda = 632.8 \text{ nm}$. The parameters for the dispersion relations of low-quartz, YAB, and KABO are compiled in Table 1.

Table 1. Dispersion relations for the optical rotatory power of low-quartz, YAB, and KABO.

Crystal	Dispersion Relation ^a		
	A (° mm)	λ ₁ (nm)	ρ ₆₃₃ ^b (° mm ⁻¹)
Low-quartz, α-SiO ₂	7.17(3)	129(1)	18.69(9)
YAB, YAl ₃ (BO ₃) ₄	1.32(2)	149(4)	3.50(6)
KABO, K ₂ Al ₂ B ₂ O ₇	0.80(1)	148(3)	2.10(3)

$$^a \rho = A/(\lambda^2 - \lambda_1^2); ^b \text{ rotatory power at } \lambda = 632.8 \text{ nm.}$$

4. Discussion

4.1. Relation between Optical Activity and Crystal Structure

From a microscopic point of view, optical activity arises from a chiral arrangement of polarizable electron density. In crystals of the enantiomorphous crystal classes, the periodicity of the atomic structure often results in helical arrangements of atoms or larger structural units such as coordination polyhedra. The geometrical characteristics of such helices have been related to the sign and magnitude of the rotatory power in a number of inorganic compounds [39,44,48]. The dispersion of the rotatory power arises from transitions between electronic states that involve those orbitals that host the optically active electron density [39]. The wavelength or energy of optically active transitions therefore contains information on the structural units that contribute to the optical activity.

The crystal structure of low-quartz is composed of [SiO₄]⁴⁻ tetrahedra that share corners to form helices along the *c* axis. Indeed, the absorption wavelength derived from the dispersion relation of the rotatory power of low-quartz (Table 1) agrees well with observed and computed energy separations of about 10 eV between occupied and unoccupied orbitals of [SiO₄]⁴⁻ tetrahedra [49]. The crystal structures of YAB and KABO are more complex. In YAB, helices of [AlO₆]⁹⁻ octahedra wind along the *c* axis and are linked to each other by planar [BO₃]³⁻ groups and slightly twisted [YO₆]⁹⁻ prisms [50]. In addition to planar [BO₃]³⁻ groups, the polyhedral framework of KABO contains tetrahedral [AlO₄]⁵⁻ groups and irregularly coordinated K⁺ cations [13]. The absorption wavelengths in the dispersion relations of both YAB and KABO compare best with predicted energy gaps between occupied and unoccupied orbitals of the [BO₃]³⁻ group with a magnitude slightly above 8 eV [4,51]. Electronic transitions in octahedral [AlO₆]⁹⁻ and tetrahedral [AlO₄]⁵⁻ groups are expected at higher energies [49,52]. We therefore conclude that the optical activity of YAB and KABO arises mainly from the arrangement of [BO₃]³⁻ groups. Since most of the polarizable electron density concentrates around oxygen atoms that are shared with other structural units, a more complete approach to explain the optical activity should take into account the crystal structure as a whole [39,44].

We further note that the dispersion of the rotatory power might provide an alternative way to estimate the intrinsic absorption edge of optically active crystals. Even small amounts of impurities or defects may cause strong absorption of light at energies below the absorption edge and may therefore mask the absorption edge in conventional spectroscopic experiments. In contrast, optically active electronic transitions follow different selection rules [39] that limit the influence of impurities on the dispersion of the rotatory power. In YAB and KABO, for example, substantial absorption of UV radiation has been observed at energies well below the expected absorption edge and is attributed to impurities of Fe³⁺ [7,8,53]. As a result, YAB and KABO crystals become effectively nontransparent at wavelengths below 170 nm and 180 nm, respectively [8,53]. Based on the dispersion of the rotatory power, however, we tentatively locate the intrinsic absorption edge at around 150 nm (Table 1), in excellent agreement with first-principle calculations on the electronic structure of the [BO₃]³⁻ group [4,51].

4.2. Changes in Sign and Magnitude of Optical Activity within YAB and KABO Crystals

Figure 5 shows sections of YAB and KABO crystals cut perpendicular to the *c* axis, i.e., perpendicular to the optical axis. The sections were viewed between crossed polarizers. To generate a visible contrast

between right- and left-handed domains, however, the analyzer was rotated to bring one type of domain into extinction, a technique also used to visualize Brazil twins in low-quartz [25,26]. In YAB (Figure 5a), domain boundaries are inclined relative to the *c* axis and appear blurred. In the KABO section, domain boundaries give rise to sharp contrasts (Figure 5b), indicating an orientation of the boundaries parallel to the *c* axis.

To demonstrate that the contrast between domains in the images indeed arises from opposing signs of optical activity, we measured the apparent rotatory power ρ^* at different locations on the crystal sections using the setup with the He-Ne laser (Section 2.3 and Figure 1b). The results are superimposed on the images as the color-coded ratio of apparent to intrinsic rotatory power $\rho^*/|\rho|$ at a wavelength of 632.8 nm. A spatial correlation exists both between domains in extinction (dark) and positive apparent rotatory powers (orange) and between bright regions and negative apparent rotatory powers (blue). Changes in sign of the apparent rotatory power across the crystal sections demonstrate the presence of right- and left-handed domains within individual YAB and KABO crystals. As proposed for YAB [18,21], we interpret these domains as inversion twins and note, to the best of our knowledge, that inversion twins have not previously been detected in KABO crystals.

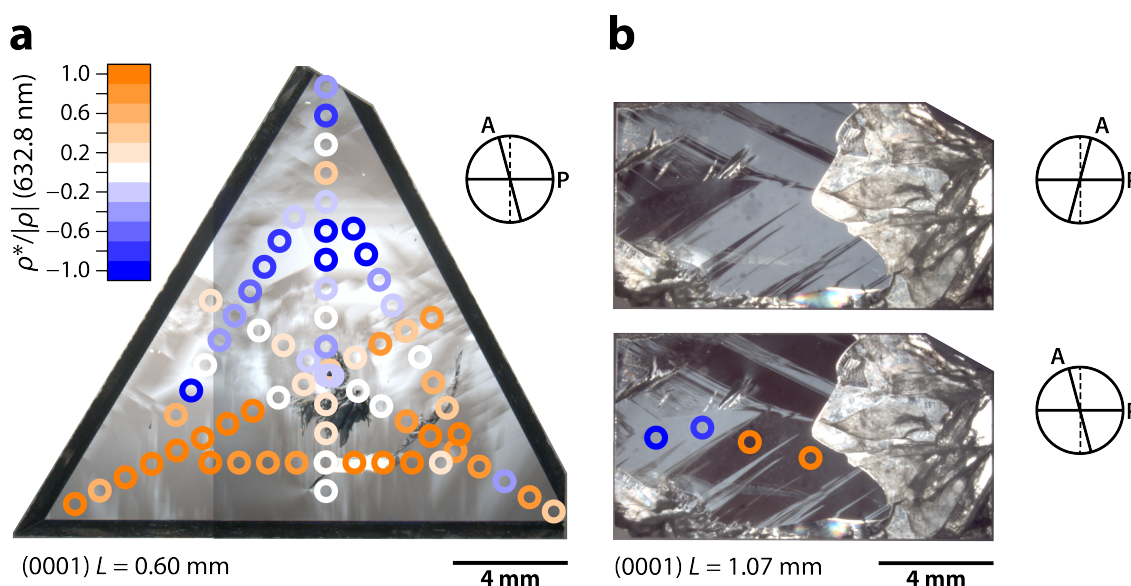


Figure 5. (a) YAB and (b) KABO crystals cut perpendicular to the *c* axis. The crystal sections are viewed between slightly decrossed polarizers as schematically indicated by the diagrams showing the relative orientations of the polarizer (P) and analyzer (A) for each image. Note the congruence of domains that are in extinction positions in the upper panel of (b) and appear bright in the lower panel and vice versa. The colored rings give the positions for measurements of the apparent rotatory power. The size of the symbols reflects the approximate diameter of the laser beam. Rings are colored according to the relative apparent rotatory power at a wavelength of 632.8 nm, as indicated by the color scale in (a). Note the correlation between the extinction behavior and the sign of the apparent rotatory power.

While dark and bright domains in the KABO section give apparent rotatory powers close to 1 and -1 , respectively, a whole range of intermediate values is observed in the YAB section. Reduced magnitudes of the apparent rotatory power are best explained by contributions of both right- and left-handed domains to the crystal volume probed by the laser beam. Fine lamellar intergrowths of the right- and left-handed domains can be found in both crystal sections (Figure 5). In the case of YAB, this microstructure most certainly corresponds to polysynthetic inversion twinning, which was reported in earlier studies using different imaging techniques [18–21,24]. Domain boundaries that are inclined with respect to the light path may also lead to a superposition of wedges with opposing signs of rotation and thereby reduce the observed rotation angle. In principle, the magnitude of

the ratio $\rho^* / |\rho|$ corresponds to the volume fraction of one type of domain within the probed crystal volume. Any quantitative estimate would require knowing the exact geometry and internal intensity distribution of the light beam inside the crystal, a task we did not attempt here. Our descriptions for the dispersion relations of the rotatory power of YAB and KABO, however, facilitate such estimates to be done at different wavelengths, offering an inexpensive and practicable method to assess the extent of inversion twinning.

Depending on the actual twin law, a pattern of domains with exactly opposing polarities can be formed in different ways. In crystal class 32, a reflection on planes perpendicular to the polar *a* axes will result in a pattern with domains of exactly opposing polarities and, at the same time, convert the right-handed polytype into the left-handed one (and vice versa). This would correspond to so-called Brazil twins in low-quartz. As with Dauphiné twins in low-quartz, domains with opposing polarities could also result from twinning by a two-fold rotation around the *c* axis. Such a two-fold rotation around the *c* axis, however, would not invert the sense of optical rotation. The domains visible in the YAB and KABO crystals shown in Figure 5 are therefore inversion twins that require reflection as twin operation. Our observations of right- and left-handed domains complement earlier analyses of the microstructure of YAB crystals that proposed reflection on $\{11\bar{2}0\}$ planes as twin operation [18,21]. This twin law generates domains with opposing polarities, and the resulting microstructure is expected to strongly affect the NLO properties of twinned YAB crystals [21,24,30].

5. Conclusions

We developed and tested a simple method to measure the rotatory power of optically active crystals at different wavelengths using a spectrophotometer with rotatable polarizers. This method was applied to determine the optical rotatory dispersion of the NLO borate crystals YAB and KABO. In both YAB and KABO, the absorption wavelengths of optically active electronic absorptions reflect the electronic structure of the $[\text{BO}_3]^{3-}$ group, suggesting that the optical activity arises mainly from the arrangement of borate groups in the crystal structures of these materials. By probing different locations in oriented crystal sections with a He-Ne laser beam, we found the sign and magnitude of the optical rotation to vary within individual YAB and KABO crystals. The variations in apparent rotatory power correlate with the microstructure of the crystals when viewed between crossed polarizers. We explain these changes in sign and magnitude of the apparent rotatory power with right- and left-handed domains that form inversion twins. In combination with proposed twin laws, such inversion twins might affect the NLO properties of YAB and KABO crystals if polar axes of adjacent domains point in opposite directions. The here-derived dispersion relations for the rotatory power of YAB and KABO facilitate fast and inexpensive assessment of the extent of inversion twinning. Based on quantitative measurements of the rotatory power, a direct measurement of the degree of twinning of the investigated crystal volume and the selection of high-quality (twin-free) crystal specimens is now possible.

Author Contributions: J.B. and V.W. designed and developed the measurement procedures; J.B. and S.D. performed measurements and analyzed data; V.W., A.G., and D.R. grew YAB and KABO crystals; V.W. and D.R. supervised and managed the project; J.B. wrote the manuscript; all authors commented on the manuscript.

Funding: This research was funded in part by the Bundesministerium für Bildung und Forschung, grant number 13N11560.

Acknowledgments: We thank B. Wenzel, M. Meiers, and A. Klintz for sample preparation and optical polishing and S. Ilas, J. Ren, J. Lejay, P. Loiseau, G. Aka, R. Maillard, and A. Maillard for enlightening discussions. K. Dupré provided a low-quartz crystal, and M. Peltz built the He-Ne laser setup for measurements of the optical activity.

Conflicts of Interest: The authors declare no conflict of interest. The funders had no role in the design of the study; in the collection, analyses, or interpretation of data; in the writing of the manuscript, or in the decision to publish the results.

Abbreviations

The following abbreviations are used in this manuscript:

BBO	β -BaB ₂ O ₄
CLBO	CsLiB ₆ O ₁₀
KABO	K ₂ Al ₂ B ₂ O ₇
KBBF	KBe ₂ BO ₃ F ₂
LBO	LiB ₃ O ₅
NLO	nonlinear optical
REE	rare-earth element
SBBO	Sr ₂ Be ₂ B ₂ O ₇
SHG	second harmonic generation
TSSG	top-seeded solution growth
UV	ultraviolet
YAB	YAl ₃ (BO ₃) ₄
YLSB	Y _{0.57} La _{0.72} Sc _{2.71} (BO ₃) ₄

References

1. Mills, A.D. Crystallographic data for new rare earth borate compounds, RX₃(BO₃)₄. *Inorg. Chem.* **1962**, *1*, 960–961. [[CrossRef](#)]
2. Ballman, A.A. A new series of synthetic borates isostructural with the carbonate mineral huntite. *Am. Mineral.* **1962**, *47*, 1380–1383.
3. Leonyuk, N.I.; Leonyuk, L.I. Growth and characterization of RM₃(BO₃)₄ crystals. *Prog. Cryst. Growth Charact.* **1995**, *31*, 179–278. [[CrossRef](#)]
4. Chen, C.; Wang, Y.; Xia, Y.; Wu, B.; Tang, D.; Wu, K.; Wenrong, Z.; Yu, L.; Mei, L. New development of nonlinear optical crystals for the ultraviolet region with molecular engineering approach. *J. Appl. Phys.* **1995**, *77*, 2268–2272. [[CrossRef](#)]
5. Becker, P. Borate materials in nonlinear optics. *Adv. Mater.* **1998**, *10*, 979–992. [[CrossRef](#)]
6. Xue, D.; Betzler, K.; Hesse, H.; Lammers, D. Nonlinear optical properties of borate crystals. *Solid State Commun.* **2000**, *114*, 21–25. [[CrossRef](#)]
7. Yu, X.; Yue, Y.; Yao, J.; Hu, Z.G. YAl₃(BO₃)₄: Crystal growth and characterization. *J. Cryst. Growth* **2010**, *312*, 3029–3033. [[CrossRef](#)]
8. Yu, J.; Liu, L.; Zhai, N.; Zhang, X.; Wang, G.; Wang, X.; Chen, C. Crystal growth and optical properties of YAl₃(BO₃)₄ for UV applications. *J. Cryst. Growth* **2012**, *341*, 61–65. [[CrossRef](#)]
9. Rytz, D.; Gross, A.; Vernay, S.; Wesemann, V. YAl₃(BO₃)₄: A novel NLO crystal for frequency conversion to UV wavelengths. In Proceedings of the Solid State Lasers and Amplifiers III SPIE, Strasbourg, France, 7–11 April 2008; Volume 6998, p. 699814. [[CrossRef](#)]
10. Chen, C.T.; Wu, B.C.; Jiang, A.D.; You, G.M. A new-type ultraviolet SHG crystal: β -BaB₂O₄. *Sci. Sin. B* **1985**, *18*, 235–243.
11. Chen, C.; Wu, Y.; Jiang, A.; Wu, B.; You, G.; Li, R.; Lin, S. New nonlinear-optical crystal: LiB₃O₅. *J. Opt. Soc. Am. B* **1989**, *6*, 616–621. [[CrossRef](#)]
12. Mori, Y.; Kuroda, I.; Nakajima, S.; Sasaki, T.; Nakai, S. New nonlinear optical crystal: Cesium lithium borate. *Appl. Phys. Lett.* **1995**, *67*, 1818–1820. [[CrossRef](#)]
13. Hu, Z.G.; Higashiyama, T.; Yoshimura, M.; Yap, Y.K.; Mori, Y.; Sasaki, T. A new nonlinear optical borate crystal K₂Al₂B₂O₇ (KAB). *Jpn. J. Appl. Phys.* **1998**, *37*, L1093. [[CrossRef](#)]
14. Ye, N.; Zeng, W.; Jiang, J.; Wu, B.; Chen, C.; Feng, B.; Zhang, X. New nonlinear optical crystal K₂Al₂B₂O₇. *J. Opt. Soc. Am. B* **2000**, *17*, 764. [[CrossRef](#)]
15. Chen, C.; Wang, Y.; Wu, B.; Wu, K.; Zeng, W.; Yu, L. Design and synthesis of an ultraviolet-transparent nonlinear optical crystal Sr₂Be₂B₂O₇. *Nature* **1995**, *373*, 322–324. [[CrossRef](#)]
16. Chen, C.; Xu, Z.; Deng, D.; Zhang, J.; Wong, G.K.L.; Wu, B.; Ye, N.; Tang, D. The vacuum ultraviolet phase-matching characteristics of nonlinear optical KBe₂BO₃F₂ crystal. *Appl. Phys. Lett.* **1996**, *68*, 2930–2932. [[CrossRef](#)]

17. Wu, B.; Tang, D.; Ye, N.; Chen, C. Linear and nonlinear optical properties of the $\text{KBe}_2\text{BO}_3\text{F}_2$ (KBBF) crystal. *Opt. Mater.* **1996**, *5*, 105–109. [[CrossRef](#)]
18. Hu, X.B.; Jiang, S.S.; Huang, X.R.; Liu, W.J.; Ge, C.Z.; Wang, J.Y.; Pan, H.F.; Ferrari, C.; Gennari, S. X-ray topographic study of twins in $\text{Nd}_x\text{Y}_{(1-x)}\text{Al}_3(\text{BO}_3)_4$ crystal. *Nuovo Cimento D* **1997**, *19*, 175–180. [[CrossRef](#)]
19. Hu, X.B.; Jiang, S.S.; Huang, X.R.; Liu, W.J.; Ge, C.Z.; Wang, J.Y.; Pan, H.F.; Jiang, J.H.; Wang, Z.G. The growth defects in self-frequency-doubling laser crystal $\text{Nd}_x\text{Y}_{1-x}\text{Al}_3(\text{BO}_3)_4$. *J. Cryst. Growth* **1997**, *173*, 460–466. [[CrossRef](#)]
20. Péter, A.; Polgár, K.; Beregi, E. Revealing growth defects in non-linear borate single crystals by chemical etching. *J. Cryst. Growth* **2000**, *209*, 102–109. [[CrossRef](#)]
21. Zhao, S.; Wang, J.; Sun, D.; Hu, X.; Liu, H. Twin structure in $\text{Yb:YAl}_3(\text{BO}_3)_4$ crystal. *J. Appl. Crystallogr.* **2001**, *34*, 661–662. [[CrossRef](#)]
22. Ye, N.; Stone-Sundberg, J.L.; Hruschka, M.A.; Aka, G.; Kong, W.; Keszler, D.A. Nonlinear optical crystal $\text{Y}_x\text{La}_y\text{Sc}_z(\text{BO}_3)_4$ ($x + y + z = 4$). *Chem. Mater.* **2005**, *17*, 2687–2692. [[CrossRef](#)]
23. Bourezzou, M.; Maillard, A.; Maillard, R.; Villeval, P.; Aka, G.; Lejay, J.; Loiseau, P.; Rytz, D. Crystal defects revealed by Schlieren photography and chemical etching in nonlinear single crystal LYSB. *Opt. Mater. Express* **2011**, *1*, 1569–1576. [[CrossRef](#)]
24. Ilas, S. Elaboration et Caractérisation de Matériaux Non-Linéaires Pour la Conception de Dispositifs Laser Émettant Dans L’ultraviolet. Ph.D. Thesis, Université Pierre et Marie Curie-Paris VI, Paris, France, 2014.
25. Schlössin, H.H.; Lang, A.R. A study of repeated twinning, lattice imperfections and impurity distribution in amethyst. *Philos. Mag.* **1965**, *12*, 283–296. [[CrossRef](#)]
26. McLaren, A.C.; Pitkethly, D.R. The twinning microstructure and growth of amethyst quartz. *Phys. Chem. Miner.* **1982**, *8*, 128–135. [[CrossRef](#)]
27. He, M.; Kienle, L.; Simon, A.; Chen, X.L.; Duppel, V. Re-examination of the crystal structure of $\text{Na}_2\text{Al}_2\text{B}_2\text{O}_7$: stacking faults and twinning. *J. Solid State Chem.* **2004**, *177*, 3212–3218. [[CrossRef](#)]
28. Giacobozzo, C.; Monaco, H.L.; Artioli, G.; Viterbo, D.; Milanese, M.; Gilli, G.; Gilli, P.; Zanotti, G.; Ferraris, G.; Catti, M. (Eds.) *Fundamentals of Crystallography*, 3rd ed.; Oxford University Press: Oxford, UK, 2011.
29. Dekker, P.; Dawes, J.M. Characterisation of nonlinear conversion and crystal quality in Nd- and Yb-doped YAB. *Opt. Express* **2004**, *12*, 5922–5930. [[CrossRef](#)]
30. Dekker, P.; Dawes, J. Twinning and “natural quasi-phase matching” in Yb:YAB. *Appl. Phys. B* **2006**, *83*, 267. [[CrossRef](#)]
31. Fejer, M.M.; Magel, G.A.; Jundt, D.H.; Byer, R.L. Quasi-phase-matched second harmonic generation: tuning and tolerances. *IEEE J. Quantum Elect.* **1992**, *28*, 2631–2654. [[CrossRef](#)]
32. Kurimura, S.; Harada, M.; Muramatsu, K.i.; Ueda, M.; Adachi, M.; Yamada, T.; Ueno, T. Quartz revisits nonlinear optics: Twinned crystal for quasi-phase matching [Invited]. *Opt. Mater. Express* **2011**, *1*, 1367. [[CrossRef](#)]
33. Ishizuki, H.; Taira, T. Quasi phase-matched quartz for intense-laser pumped wavelength conversion. *Opt. Express* **2017**, *25*, 2369. [[CrossRef](#)]
34. Liu, H.; Li, J.; Fang, S.H.; Wang, J.Y.; Ye, N. Growth of $\text{YAl}_3(\text{BO}_3)_4$ crystals with tungstate based flux. *Mater. Res. Innov.* **2011**, *15*, 102–106. [[CrossRef](#)]
35. Zhang, C.; Wang, J.; Hu, X.; Liu, H.; Wei, J.; Liu, Y.; Wu, Y.; Chen, C. Top-seeded growth of $\text{K}_2\text{Al}_2\text{B}_2\text{O}_7$. *J. Cryst. Growth* **2001**, *231*, 439–441. [[CrossRef](#)]
36. Zhang, C.; Wang, J.; Hu, X.; Jiang, H.; Liu, Y.; Chen, C. Growth of large $\text{K}_2\text{Al}_2\text{B}_2\text{O}_7$ crystals. *J. Cryst. Growth* **2002**, *235*, 1–4. [[CrossRef](#)]
37. Nye, J.F. *Physical Properties of Crystals: Their Representation by Tensors and Matrices*; Oxford University Press: Oxford, UK, 1985; p. 352.
38. Haussühl, S. *Physical Properties of Crystals: An Introduction*; Wiley-VCH: Weinheim, Germany, 2007; p. 453.
39. Glazer, A.M.; Stadnicka, K. On the origin of optical activity in crystal structures. *J. Appl. Crystallogr.* **1986**, *19*, 108–122. [[CrossRef](#)]
40. Dimitriu, D.G.; Dorohoi, D.O. New method to determine the optical rotatory dispersion of inorganic crystals applied to some samples of Carpathian Quartz. *Spectrochim. Acta Part A* **2014**, *131*, 674–677. [[CrossRef](#)] [[PubMed](#)]

41. Dorohoi, D.O.; Dimitriu, D.G.; Cosutchi, I.; Breaban, I.; Closca, V. A new method for determining the optical rotatory dispersion of transparent crystalline layers. In Proceedings of the Second International Conference on Applications of Optics and Photonics, Aveiro, Portugal, 26–30 May 2014; Volume 9286, p. 92862Z. [[CrossRef](#)]
42. Jiang, S.; Jia, H.; Lei, Y.; Shen, X.; Cao, J.; Wang, N. Novel method for determination of optical rotatory dispersion spectrum by using line scan CCD. *Opt. Express* **2017**, *25*, 7445–7454. [[CrossRef](#)] [[PubMed](#)]
43. Lowry, T.M. *Optical Rotatory Power*; Longmans: London, UK, 1935.
44. Devarajan, V.; Glazer, A.M. Theory and computation of optical rotatory power in inorganic crystals. *Acta Crystallogr. A* **1986**, *42*, 560–569. [[CrossRef](#)]
45. Chandrasekhar, S. Optical rotatory dispersion of crystals. *Proc. R. Soc. Lond. Ser. A* **1961**, *259*, 531–553. [[CrossRef](#)]
46. Lowry, T.M.; Coode-Adams, W.R.C.X. Optical rotatory dispersion. Part III.—The rotatory dispersion of quartz in the infra-red, visible and ultra-violet regions of the spectrum. *Philos. Trans. R. Soc. A* **1927**, *226*, 391–466. [[CrossRef](#)]
47. Katzin, L.I. The rotatory dispersion of quartz. *J. Phys. Chem.* **1964**, *68*, 2367–2370. [[CrossRef](#)]
48. Ramachandran, G.N. Theory of optical activity of crystals. In *Proceedings of the Indian Academy of Sciences-Section A*; Indian Academy of Sciences: Bengaluru, India, 1951; Volume 33, pp. 217–227. [[CrossRef](#)]
49. Tossell, J.A. Electronic structures of silicon, aluminum, and magnesium in tetrahedral coordination with oxygen from SCF- $X\alpha$ MO calculations. *J. Am. Chem. Soc.* **1975**, *97*, 4840–4844. [[CrossRef](#)]
50. Belokoneva, E.L.; Azizov, A.V.; Leonyuk, N.I.; Simonov, M.A.; Belov, N.V. Crystal structure of $YAl_3[BO_3]_4$. *J. Struct. Chem.* **1981**, *22*, 476–478. [[CrossRef](#)]
51. Tossell, J.A. Studies of unoccupied molecular orbitals of the B–O bond by molecular orbital calculations, X-ray absorption near edge, electron transmission, and NMR spectroscopy. *Am. Mineral.* **1986**, *71*, 1170–1177.
52. Tossell, J.A. The electronic structures of Mg, Al and Si in octahedral coordination with oxygen from SCF $X\alpha$ MO calculations. *J. Phys. Chem. Solids* **1975**, *36*, 1273–1280. [[CrossRef](#)]
53. Liu, L.; Liu, C.; Wang, X.; Hu, Z.G.; Li, R.K.; Chen, C.T. Impact of Fe^{3+} on UV absorption of $K_2Al_2B_2O_7$ crystals. *Solid State Sci.* **2009**, *11*, 841–844. [[CrossRef](#)]



© 2018 by the authors. Licensee MDPI, Basel, Switzerland. This article is an open access article distributed under the terms and conditions of the Creative Commons Attribution (CC BY) license (<http://creativecommons.org/licenses/by/4.0/>).